Available online at www.sciencedirect.com
ScienceDirect
Earth and Planetary Science Letters 255 (2007) 53–69
EPSL
www.elsevier.com/locate/epsl

Constraints on mantle melting and composition and nature of slab components in volcanic arcs from volatiles (H_2O, S, Cl, F) and trace elements in melt inclusions from the Kamchatka Arc

Maxim Portnyagin [a,b,*], Kaj Hoernle [a], Pavel Plechov [c], Nikita Mironov [b], Sergey Khubunaya [d]

[a] *IFM-GEOMAR Leibniz Institute for Marine Sciences at the University of Kiel, Wischhofstrasse 1-3, 24148 Kiel, Germany*
[b] *Vernadsky Institute, Kosygin 19, 119991 Moscow, Russia*
[c] *Moscow State University, Department of Geology, 119899 Moscow, Russia*
[d] *Institute of Volcanology and Seismology, Piip 9, 683006 Petropavlovsk-Kamchatsky, Russia*

Received 19 June 2006; received in revised form 4 December 2006; accepted 5 December 2006
Available online 19 January 2007
Editor: R.W. Carlson

Abstract

New and published data on the composition of melt inclusions in olivine ($Fo_{73–91}$) from volcanoes of the Kamchatka and northern Kurile Arc are used 1) to evaluate the combined systematics of volatiles (H_2O, S, Cl, F) and incompatible trace elements in their parental magmas and mantle sources, 2) to constrain thermal conditions of mantle melting, and 3) to estimate the composition of slab-derived components. We demonstrate that typical Kamchatkan arc-type magmas originate through 5–14% melting of sources similar or slightly more depleted in HFSE (with up to ~1 wt.% previous melt extraction) compared to MORB-source mantle, but strongly enriched in H_2O, B, Be, Li, Cl, F, LILE, LREE, Th and U. Mean H_2O in parental melts (1.8–2.6 wt.%) decreases with increasing depth to the subducting slab and correlates negatively with both 'fluid-immobile' (e.g. Ti, Na, LREE) and most 'fluid-mobile' (e.g. LILE, S, Cl, F) incompatible elements, implying that solubility in hydrous fluids or amount of water does not directly control the abundance of 'fluid-mobile' incompatible elements. Strong correlation is observed between H_2O/Ce and B/Zr (or B/LREE) ratios. Both, calculated H_2O in mantle sources (0.1–0.4%) and degrees of melting (5–14%) decrease with increasing depth to the slab indicating that the ultimate source of water in the sub-arc mantle is the subducting oceanic plate and that water flux (together with mantle temperature) governs the extent of mantle melting beneath Kamchatka. A parameterized hydrous melting model [Katz et al. 2003, G^3, 4(9), 1073] is utilized to estimate that mantle melting beneath Kamchatka occurs at or below the dry peridotite solidus (1245–1330 °C at 1.5–2.0 GPa). Relatively high mantle temperatures (yet lower than beneath back-arc basins and ocean ridges) suggest substantial corner flow driven mantle upwelling beneath Kamchatka in agreement with numerical models implying non-isoviscous mantle wedge rheology. Data from Kamchatka, Mexico and Central America indicate that <5% melting would take place beneath continental arcs without water flux from the subducting slab. A broad negative correlation appears to exist between crustal thickness and the temperature of magma generation beneath volcanic arcs with larger amounts of decompression melting occurring beneath thinner arc crust (lithosphere). In agreement with the high mantle temperatures, we observe a systematic change in the composition of slab components with increasing slab depth from solute-poor hydrous fluid beneath the volcanic front to solute-rich hydrous melt or supercritical liquid at deeper depths beneath the rear arc. The solute-rich slab component dominates the budget of LILE, LREE, Th

* Corresponding author. IFM-GEOMAR Leibniz Institute for Marine Sciences at the University of Kiel, Wischhofstrasse 1-3, 24148 Kiel, Germany.
E-mail address: mportnyagin@ifm-geomar.de (M. Portnyagin).

0012-821X/$ - see front matter
doi:10.1016/j.epsl.2006.12.005

and U in the magmas and originates through wet-melting of subducted sediments and/or altered oceanic crust at ≥120 km depth. Melting of the upper parts of subducting plates under water flux from deeper lithosphere (e.g. serpentinites), combined with high temperatures in the mantle wedge, may be a more common process beneath volcanic arcs than has been previously recognized.

Keywords: subduction zone magmatism; water; volatiles; trace elements; decompression; hydrous melting; Kamchatka volcanism

1. Introduction

Water-rich fluids and melts released from descending oceanic plates are thought to play a key role in subduction zone (SZ) magmatism as they can transfer material from the subducting plate to the overlying mantle wedge, lowering the solidus of mantle peridotite and triggering partial melting [1–4]. Pressure-release melting at temperatures above dry peridotite solidus has also been proposed to take place above SZs [3,5–8]. In essence, elucidating relative contributions from flux versus decompression melting in SZs is a fundamental question concerning the thermal state of the mantle wedge. Due to the scarcity of accurate data on water contents in primitive arc magmas, the thermal conditions of magma generation are difficult to constrain.

Melt inclusions in phenocrysts – small pockets of melt trapped in crystals and thus isolated from further evolution of the host magma – provide a unique opportunity to study undegassed arc magmas, since they can (under favourable circumstances) preserve near primary volatile contents of primitive arc melts (e.g. [9,10]). The compositions of primitive melt inclusions in arc rocks, thus, allows us to address several fundamental, and possibly inter-related, questions about arc magmatism and the dynamics of SZs, including the thermal state of the mantle wedge, partial melting regime, magnitude of mantle upwelling, and the composition and nature of slab-derived components. In this study, we address these questions using new data on volatile (H_2O, S, Cl, F) and trace element contents in primitive melt inclusions from the Kamchatka Arc, one of the most active volcanic arcs on Earth.

2. Kamchatka Arc and studied samples

The Kamchatka Arc in the northwestern part of the Pacific 'Ring of Fire' is an area of high seismic activity and abundant volcanism related to fast (7.6–7.8 cm/y) subduction of the 80–100 My old Pacific Plate beneath the Eurasian continental margin [11]. The subduction dip angle at 100–200 km depth (region of magma generation) is ~55° beneath southern Kamchatka and becomes as shallow as ~30° near the Kamchatka–Aleutian junction, where subduction beneath Kamchatka appears to terminate.

Quaternary volcanism in Kamchatka developed within two major volcanic zones: Eastern Volcanic Belt (EVB) and Sredinny Range (Fig. 1). Detailed geologic description of the volcanic zones can be found elsewhere [12]. Our study focused on the EVB, which accommodates the majority of active volcanoes in Kamchatka. In its southern and central parts, the EVB is an ~100 km wide volcanic belt, including a volcanic front (VF), a chain of large polygenetic volcanoes located 100–140 km above the subducting slab, and rear arc (RA), consisting of large volcanoes and smaller monogenetic volcanic edifices located up to 200 km above the slab and up to 100 km behind the VF. The northern part of the EVB extends into the Central Kamchatka Depression (CKD). Here the subducted slab is located at depths 150–200 km beneath the Klyuchevskoy Group of volcanoes, containing the world's most productive arc volcanoes, and shallows to ~100 km beneath the Shiveluch Volcano, the northernmost active volcano in Kamchatka.

For this melt inclusion study, we selected 9 samples from the entire EVB (Supplementary Table 1). In order to assess the composition of primitive magmas, we focused the study exclusively on rocks containing large (0.5–20 mm) olivine phenocrysts, which were among the most primitive in Kamchatka olivine±clinopyroxene± plagioclase basalts and basaltic andesites with Mg#=54–71 mol% (Mg#=100*MgO/(MgO+FeO) calculated on molar basis). All rocks represent historic to Holocene eruptions and provide information about the present-day magma generation. VF samples were collected from Ksudach (Holocene deposits) and Karymsky (1996 A.D. eruption) volcanoes. Farafonova Pad′ (~1500 B.P.) volcanic field represents RA volcanism. CKD samples are from Tolbachik volcano (1004 cone, 1000–1500 B.P.), from pre-historic (Bulochka and Luchitsky cones, ~2800 B.P.) and historic (Apakhonchich, 1945 A.D. and Piip, 1966 A.D.) eruptions of Klyuchevskoy volcano. The samples ranged from lavas, volcanic bombs and scoria to intrusive segregations of large (up to 1 cm) olivine and plagioclase crystals known as 'allivalites' [13]. In general, the most primitive samples hosting high-Fo olivine (up to Fo_{91}) come from RA and CKD volcanoes (Supplementary Fig. 1). VF samples (Ksudach, Karymsky) are more evolved and contain relatively

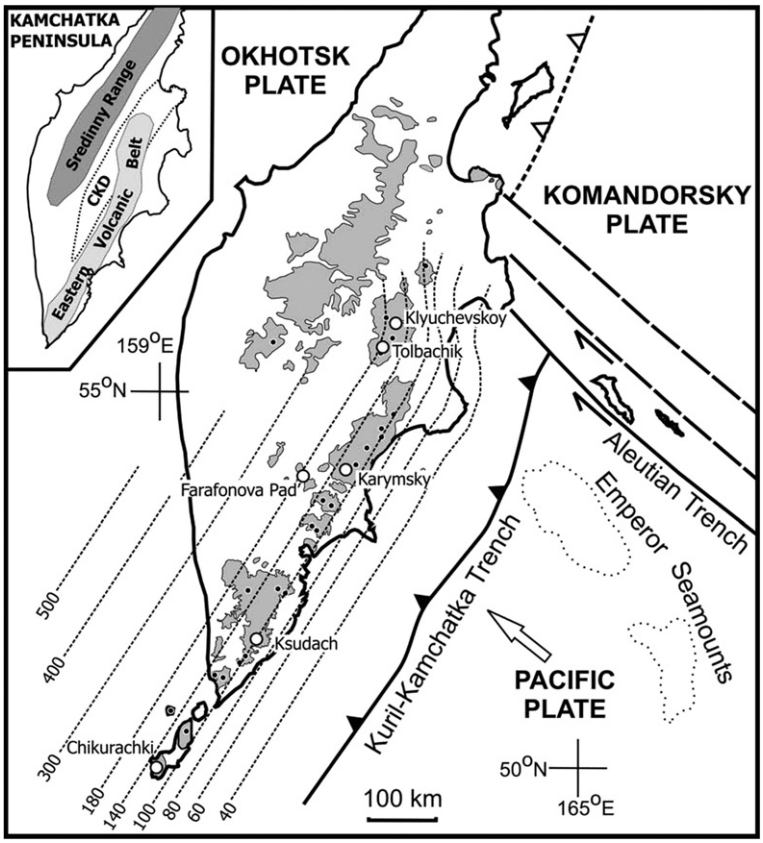

Fig. 1. Major volcanic zones of the Kamchatka Arc [12]. Studied volcanoes are denoted with open circle. Distribution of Quaternary volcanics is shown by dark gray pattern. Dashed lines indicate depths to the subducting Pacific slab [11]. The Central Kamchatka Depression (CKD) is a rift-like tectonic structure between the Eastern Volcanic Belt (EVB) and Sredinny Ranges of Kamchatka. Northern part of the EVB is shifted to the west and located within the CKD, possibly in part reflecting shallower subduction angle where the Emperor Seamount chain is subducting. Southern part of the CKD is not volcanically active.

Fe-rich olivine (<Fo_{85}), for which parental melt compositions were extrapolated.

For the sake of comparison and to increase the number of samples which are well characterized for volatile and trace elements, we include in our study recently published data on the composition of melt inclusions in olivine from Chikurachki volcano on Paramushir Island [14]. The island is located ~50 km south of the southern tip of Kamchatka and belongs to the northern Kuril Arc, which has the same structure and history of volcanism as the southern segment of the Kamchatka Arc.

3. Methods

3.1. Experimental and analytical methods

About two thirds of the 60 melt inclusions studied were partially re-crystallized at room temperature and required experimental re-heating prior to analysis for composition of trapped melt. Rapid (<5 min) re-heating experiments were carried out at the Vernadsky Institute (Moscow) and at the Geologic Department of the Moscow State University following techniques reported elsewhere [9,15]. Subsequent comparison of re-heated and natural glassy inclusions from the same sample (Apakhonchich flow of Klyuchevskoy volcano) revealed no systematic differences in concentrations of volatile and incompatible trace elements between inclusions directly measured and those that required re-heating prior to analyses. Major elements, S and Cl in glasses of melt inclusions and in olivine were analyzed by Camebax microbeam and Cameca SX100 electron microprobes at the Vernadsky Institute (Moscow) and Cameca SX50 electron microprobe at IFM-GEOMAR (Kiel). Concentrations of water, F and 23 trace elements were determined by secondary ion mass-spectrometry (SIMS) using a CAMECA ims4f at Institute of Microelectronics (Yaroslavl′, Russia). Details of experimental and analytical techniques can be found in Supplementary methods, and the complete major element, trace element

Table 1
Mean compositions of melt inclusions, parental melts, melting parameters and slab components

Region	Kamchatka	N. Kurile Arc	Kamchatka	Kamchatka	Kamchatka	Kamchatka	Kamchatka
Volcano	Ksudach	Chikurachki	Karymsky	Farafonova Pad'	Tolbachik	Klyuchevskoy historic	Klyuchevskoy pre-historic
Volcanic zone [a]	VF	VF	VF	RA	CKD	CKD	CKD
Depth to slab (km) [b]	100	120	125	175	180	160	160
Dist. from trench (km)	200	230	230	280	250	230	230
Number inclusions	4	14	6	5	11	14	15
Fo range (mol%)	81.0–76.6	75.1–72.4	81.8–72.0	89.2–87.7	90.8–88.0	90.1–79.4	90.6–87.5
Melt inclusions corrected for Fe-loss [c]							
SiO_2 (wt.%)	50.61±1.24	52.65±1.50	52.94±1.73	45.73±0.83	47.23±0.43	49.22±1.28	48.99±1.05
TiO_2 (wt.%)	0.88±0.03	1.06±0.15	0.92±0.06	1.15±0.07	0.88±0.10	0.96±0.13	0.86±0.08
Al_2O_3 (wt.%)	15.53±0.40	16.38±0.63	16.21±0.69	17.36±0.60	12.49±0.86	16.03±1.58	14.60±0.68
FeO (wt.%)	9.84±0.05	10.64±0.53	9.21±0.86	8.73±0.11	9.63±0.05	8.24±0.10	8.34±0.03
MnO (wt.%)	0.32±0.04	0.23±0.02	0.15±0.03	0.12±0.03	0.16±0.02	0.11±0.03	0.11±0.02
MgO (wt.%)	5.92±0.69	4.57±0.30	5.53±1.10	9.47±0.49	11.66±0.93	8.36±1.88	10.07±0.83
CaO (wt.%)	11.35±0.25	8.40±0.37	8.05±0.95	12.52±0.70	12.27±0.50	10.80±1.44	11.60±1.20
Na_2O (wt.%)	1.83±0.12	2.77±0.31	2.86±0.17	2.73±0.13	2.10±0.23	3.00±0.48	2.56±0.29
K_2O (wt.%)	0.18±0.01	0.76±0.07	0.70±0.14	0.54±0.04	0.65±0.05	0.84±0.22	0.49±0.11
P_2O_5 (wt.%)		0.23±0.03	0.17±0.05		0.17±0.02	0.17±0.03	0.13±0.03
Cl (wt.%)	0.09±0.02	0.10±0.01	0.09±0.03	0.11±0.01	0.09±0.01	0.09±0.02	0.07±0.02
S (wt.%)	0.10±0.05	0.13±0.04	0.15±0.05	0.28±0.02	0.24±0.04	0.20±0.05	0.16±0.05
H_2O (wt.%)	3.35±0.17	3.23±0.33	3.02±0.59	2.08±0.67	2.42±0.51	1.97±0.54	2.04±0.46
Parental melts [d]							
Olivine added (mol%)	16.0–19.8	22.0–24.8	13.5–23.0	1.6–4.9	0–4.6	0–14.6	0–5.7
TiO_2 (wt.%)	0.68±0.05	0.75±0.11	0.73±0.05	1.11±0.06	0.86±0.11	0.90±0.10	0.84±0.07
Na_2O (wt.%)	1.42±0.07	1.95±0.23	2.28±0.22	2.63±0.10	2.06±0.25	2.80±0.35	2.50±0.24
K_2O (wt.%)	0.13±0.01	0.53±0.05	0.56±0.08	0.52±0.04	0.63±0.10	0.78±0.20	0.48±0.10
H_2O (mean) (wt.%)	2.60±0.10	2.27±0.24	2.41±0.36	2.03±0.69	2.37±0.50	1.84±0.41	1.98±0.41
H_2O (maximum) (wt.%)	2.71	2.48	2.75	2.61	2.81	2.69	2.70
Cl (ppm)	678±124	703±72	701±203	1084±132	913±99	884±210	682±203
S (ppm)	773±440	896±268	1111±371	2716±201	2309±368	1870±433	1524±456
Li (ppm)	3.76±0.48	5.12±0.76	5.24±1.05	4.11±0.20	4.75±0.20	6.43±1.59	4.64±0.87
Be (ppm)	0.24±0.02	0.35±0.04	0.52±0.05	0.59±0.05	0.67±0.12	0.50±0.07	0.39±0.04
B (ppm)	13.0±1.8	12.3±0.5	6.0±0.8	6.1±0.5	9.9±0.9	11.2±1.0	12.7±2.0
F (ppm)	99±33		219±39	328±94	400±124	401±130	254±40
Y (ppm)	14.2±1.1	17.3±1.8	14.7±1.3	25.3±2.8	18.8±1.2	17.6±1.5	16.6±1.4
Zr (ppm)	24.1±3.3	42.3±4.3	58.3±8.6	75.7±9.3	64.0±1.9	64.6±7.2	53.0±9.1
Sr (ppm)	212±21	296±26	306±38	395±34	303±4	304±26	238±22
Nb (ppm)	0.52±0.19	0.98±0.13	1.73±0.21	1.76±0.30	1.89±0.26	1.55±0.35	1.14±0.22
Ba (ppm)	51±3	146±7	179±20	148±9	249±26	270±58	188±27
La (ppm)	1.9±0.3	4.7±0.3	5.3±0.6	5.6±0.1	6.6±0.6	5.3±0.5	3.7±1.0
Ce (ppm)	5.9±1.4	11.6±0.7	13.5±1.3	15.8±0.3	16.4±0.7	13.7±1.3	10.1±2.7
Nd (ppm)	4.7±0.7	8.2±0.6	9.0±0.7	11.6±0.6	12.2±0.6	10.0±0.7	7.7±1.0
Sm (ppm)	1.7±0.3	2.3±0.2	2.5±0.3	3.5±0.3	3.2±0.2	2.9±0.3	2.3±0.2
Eu (ppm)	0.65±0.04	0.76±0.11	0.88±0.12	1.13±0.11	1.16±0.16	0.88±0.18	0.72±0.15
Gd (ppm)	2.01±0.03	2.87±0.30	2.88±0.25	1.13±0.73	2.85±0.50	3.40±0.28	2.65±0.25
Dy (ppm)	2.23±0.03	3.01±0.30	2.60±0.25	4.06±0.73	2.63±0.50	3.05±0.28	2.75±0.25
Er (ppm)	1.63±0.19	1.93±0.27	1.79±0.19	4.09±0.47	2.08±0.11	1.92±0.21	1.84±0.16
Yb (ppm)	1.79±0.14	1.90±0.16	1.76±0.25	2.72±0.12	1.95±0.18	1.80±0.23	1.76±0.19
Hf (ppm)	1.02±0.08	1.32±0.63	1.81±0.26	2.56±0.20	1.90±0.04	1.99±0.40	1.53±0.16
Th (ppm)	0.13±0.03	0.80±0.09	0.55±0.10	0.54±0.03	0.52±0.07	0.43±0.07	0.27±0.06
U (ppm)	0.08±0.02	–	0.35±0.08	0.28±0.04	0.27±0.08	0.30±0.05	0.19±0.05
Melting parameters							
PME (wt.%) [e]	0.91±0.50	0.46±0.14	0.02±0.02	0.72±0.21	0.07±0.06	0.20±0.13	0.32±0.11
F^m (wt.%) [f]	14.2±2.3	10.7±2.0	13.5±2.4	4.6±1.3	9.9±1.0	10.3±2.2	11.2±1.5

Table 1 (*continued*)

Region	Kamchatka	N. Kurile Arc	Kamchatka	Kamchatka	Kamchatka	Kamchatka	Kamchatka
Volcano	Ksudach	Chikurachki	Karymsky	Farafonova Pad'	Tolbachik	Klyuchevskoy historic	Klyuchevskoy pre-historic
Melting parameters							
H_2O^S (wt.%)[g]	0.40±0.06	0.27±0.06	0.35±0.05	0.13±0.06	0.26±0.07	0.21±0.07	0.24±0.06
H_2O^S (max) (wt.%)	0.41	0.29	0.40	0.15	0.31	0.31	0.33
Slab components[h]							
Amount in source (wt.%)	0.42±0.06	0.33±0.06	0.42±0.07	0.15±0.07	0.33±0.11	0.29±0.08	0.29±0.07
Ba (ppm)	1739±132	4797±313	5629±558	5290±1541	8446±1675	9704±2067	7319±1447
U (ppm)	2±1		10±3	10±5	8±2	8±5	7±2
Th (ppm)	4±1	26±2	15±2	18±7	15±2	14±3	9±3
K_2O (wt.%)	4.2±0.4	17.0±1.6	16.6±1.2	18.0±5.3	21.7±7.5	27.5±8.6	17.6±3.3
Cl (wt.%)	2.4±0.4	2.4±0.3	2.3±0.5	4.1±1.3	3.1±1.2	3.3±1.0	2.8±1.1
La (ppm)	37±6	113±9	125±24	128±39	169±27	134±26	87±27
Be (ppm)	5±1	8±2	12±1	13±4	19±10	12±2	10±2
H_2O (wt.%)	93±0	80±2	80±1	77±7	74±9	68±9	79±4
Ce (ppm)	99±49	267±14	330±65	396±123	443±98	339±118	236±83
Sr (ppm)	6624±771	9198±1071	9431±2723	14930±5351	9718±2783	10313±1800	8131±1618
Nd (ppm)	56±26	147±26	184±41	236±63	306±52	227±42	152±46
F (wt.%)	0.2±0.1		0.6±0.2	0.9±0.2	2.2±1.2	1.4±0.8	0.9±0.3
B (ppm)	517±77	489±26	217±14	307±108	425±174	497±85	594±108
Sm (ppm)	16±13	28±8	38±11	61±26	68±22	54±12	35±13
Eu (ppm)	7±2	5±5	12±4	10±7	23±13	9±7	0
Gd (ppm)	0	26±16	32±11	0	16±14	0	0
Li (ppm)	27±19	62±42	68±46	0	20±14	114±74	0
$NaCl_{eq}$ (wt.%)[i]	4.0	4.7	4.5	8.0	6.4	7.4	5.5

[a] Volcanic zones: VF—volcanic front RA—rear-arc, CKD—Central Kamchatka Depression.
[b] Depth to the subducting slab after [25].
[c] Melt inclusions were re-calculated to equilibrium with host olivine as explained in Section 3.2. Possible amount of Fe-loss from inclusions due to low-temperature re-equilibrium with host olivine was taken into account following [32].
[d] Concentrations of incompatible elements in parental melts in equilibrium with olivine Fo_{90}.
[e] PME ("Previous Melt Extraction") — amount of melt extracted from the E-DMM [44] prior melting beneath Kamchatka.
[f] F^m — degree of mantle source melting.
[g] H_2O^S — amount of H_2O in the mantle source.
[h] Composition of hydrous slab component added to mantle source during melting calculated from mean estimated H_2O concentrations in primary melts.
[i] Salinity of the slab component calculated from H_2O/Cl and expressed as NaCl equivalent. Error (±) refers to 1 S.D. of the mean values.

and volatile data set for the melt inclusions in Supplementary Table 2. Mean compositions of melt inclusions are presented in Table 1.

3.2. Correction of melt inclusions for post-entrapment modification

Most melt inclusions in magnesian olivine (Fo > 80 mol%) and some inclusions in more Fe-rich olivines, glassy or quenched during the experiment, have FeO up to 4 wt.% lower than in their host rocks, suggesting substantial re-equilibration with olivine after entrapment in olivine upon slow cooling prior to eruption [16]. The inclusions were corrected for equilibrium with the host olivines by reverse modeling of Fe–Mg exchange and olivine crystallization using computer software "Fe-loss" [16]. Initial FeO in the inclusions was assumed to equal FeO in their host rocks. Ferrous/ferric ratios in melts (Fe^{2+}/Fe^{3+} = 6–10) were estimated from compositions of coexisting chromium spinel inclusions in olivine from the same samples as described elsewhere [17]. Glassy inclusions in olivines with Fo ≤ 82 mol% from Karymsky and Chikurachki volcanoes had FeO contents similar to or slightly higher than the host rocks. These inclusions were most likely trapped shortly before eruption and thus did not re-equilibrate significantly with the host olivines. Initial composition of these inclusions was calculated by incremental (0.1 wt.%) addition of olivine until achieving the equilibrium with the host mineral. The modeling has been carried out with the help of the PETROLOG 2.1 software [15]. Uncertainty in the

determination of initial FeO content in trapped melts (±1 wt.%) was estimated to introduce ~5% relative uncertainty in calculated concentrations of incompatible elements which is small compared to the analytical uncertainty and large regional variability of melt inclusions.

3.3. Estimation of parental melts from compositions of melt inclusions

We assume that parental melts in Kamchatka were initially in equilibrium with typical mantle olivine Fo_{90}. Composition of the olivines hosting inclusions is however highly scattered from Fo_{73} to $Fo_{90.5}$ implying that most melts have experienced variable amounts of crystallization prior to trapping in olivine crystals. In order to make the compositions of melt inclusions directly comparable and to assess compositions of near primary melts, we calculated the compositions of melt inclusions in equilibrium with olivine Fo_{90} by simulating reverse fractional olivine crystallization at Ni–NiO oxygen fugacity with the help of PETROLOG 2.1. Trace elements were assumed perfectly incompatible to olivine. Mean compositions of the estimated parental melts are shown in Table 1.

Similar numerical procedure has been applied previously to estimate parental compositions of moderately fractionated back-arc melts [3,18] and thus our data is directly comparable with the results of these previous workers. We, however, realize that the approach applied does not fully account for possible effects of fractional crystallization on concentrations of incompatible elements in Kamchatkan magmas, because these magmas were likely saturated in both olivine and at least high-Ca pyroxene at the moment of trapping. Melts trapped in olivine Fo<80 mol% could also have crystallized some plagioclase. Because real average concentrations of MgO and FeO in the bulk crystallizing assemblage are lower compared to pure-olivine crystallization, estimated degrees of crystallization from parental melts, varying from ~2–7% for CKD and up to 23% for VF melts (Table 1), should be considered as minimum values and accordingly concentrations of highly incompatible elements in parental melts represent maximum values. The normalization procedure introduces a small uncertainty when recalculating inclusions in high-Fo (>85 mol%) olivine (CKD, RA), but the initial concentrations of highly incompatible elements could be overestimated by 30–40 rel.% for inclusions in evolved olivines (Fo_{72-82}) from VF melts (Ksudach, Chikurachki, Karymsky). Presently we are unable to quantitatively account for this uncertainty, and thus consider the estimates as our best possible solution, which can be potentially improved by studying inclusions in high-Fo olivines and behavior of variably incompatible elements during crystal fractionation.

Estimates of H_2O and other volatiles in parental melts can be significantly compromised by melt degassing prior to trapping in olivine, causing these estimates to be too low [10]. Since H_2O has a large effect on the liquidus temperature of major silicate minerals in basaltic systems, substantial H_2O degassing should cause massive crystallization (e.g. [19]). The majority of studied melt inclusions (CKD, RA) were, however, trapped in high-Fo (>85 mol%) and represent primitive melts, which experienced only minor crystal fractionation. Furthermore, volatile components in melt inclusions from single samples do not decrease with decreasing forsterite content of olivine, precluding coupled processes of magmatic degassing and crystallization. Melt inclusions from the VF were trapped in relatively low-Fo olivines (<81 mol%), and thus magmatic degassing during an earlier stage of evolution cannot be completely ruled out for these melts on the basis of petrological criteria. These VF inclusions, however, have the highest H_2O contents of all studied inclusions (up to 3.9 wt.%). If any H_2O loss occurred before trapping, initial H_2O concentrations in VF parental melts could have been even higher than in our estimates, reinforcing the major conclusions of our study. Contents of CO_2 and S in melt inclusions can also be used to help assess if the melts are degassed (e.g., [10]). Although we did not measure CO_2, all but 9 out of 70 inclusions reported here have high S (>1000 ppm), which is typically associated with high CO_2 (>150 ppm) in arc inclusions [20–22]. The high S contents suggest that most melts did not experience significant pre-entrapment H_2O degassing. Therefore, both petrological and geochemical evidence suggests that magmatic degassing had little (if any) effect on H_2O contents in melt inclusions.

Later processes disturbing H_2O content in melt inclusions are related to re-equilibration of melt inclusions with external conditions and can occur during subsequent evolution of the magmatic system and during experimental re-heating [15,23,24]. Experimental reheating is often claimed as the major reason of H_2O loss from inclusions due to fast dissipation of hydrogen and/or hydroxyl from inclusion through host olivine [15,25,26]. Rapid re-heating (<3 min at T>1000 °C) was applied to the inclusions studied here. Comparison of H_2O in re-heated and naturally quenched inclusions from the same samples (e.g. AP1 from Klyuchevskoy volcano) did not reveal any systematic difference

between these inclusions. H_2O content in both groups varies substantially (1.3–3 wt.%) and does not correlate with Fo or trace elements. Therefore, we conclude that either this variability reflects natural heterogeneity of parental melts or H_2O content in melt inclusions was disturbed in nature. Natural processes include H_2O loss from inclusions during transport to surface, eruption and lava cooling *and* H_2O gain in inclusions from surrounding magma, if H_2O pressure in magma exceeded that inside inclusion [23,27]. These processes of possible H_2O loss or gain in melt inclusions occurring at magmatic conditions are poorly studied and seem difficult to trace with any independent geochemical criteria. Because of this ambiguity, equally applicable to all melt inclusions in olivine, we report here mean and maximum initial water contents in parental melts determined for each volcano/lava flow (Table 1). If any kind of degassing has affected the volatile contents in at least some of the melt inclusions, then the mean calculated initial volatile contents represent minimum contents for the parental melts.

Finally, despite the serious problems associated with determining accurate volatile contents from melt inclusions, we observe geochemically reasonable correlations of mean H_2O content in parental melts with trace element contents and ratios (e.g., H_2O/Ce, B/(REE, HFSE), Nb/Y and La/Yb), as described below (see also Fig. 4). These correlations are not consistent with significant H_2O loss or gain from magmas or melt inclusions, since H_2O loss or gain would disturb such correlations, and suggest that estimated parental melts are close to true values.

4. Composition of parental melts

Mean compositions of parental melts inferred from melt inclusions have basaltic compositions and exhibit large variations in incompatible trace elements and their ratios. The patterns of trace elements normalized to Depleted MORB-source Mantle (DMM [28]) are typical for arc-type magmas (Fig. 2). These arc-type features include relative high field strength element (HFSE, e.g. Nb and Zr) depletion and strong (up to 1000 times) to moderate enrichment in H_2O, B, Cl, Li, large ion lithophile elements (LILE, e.g., Sr, K, Ba), Th and U relative to REE and HFSE of similar incompatibility.

Absolute concentrations of most incompatible elements correlate with each other in parental magmas of Kamchatka and increase systematically with increasing depth of the subducting slab (Fig. 3). The lowest concentrations are observed for VF (Ksudach) volcanoes at slab depths of ~100 km and the largest for RA and CKD volcanoes at deeper (160–180 km) depths. The largest variability was found for highly incompatible lithophile elements (e.g., Ba, Th, Nb, La) and the smallest for moderately incompatible lithophile elements (e.g., Ti, Y and HREE). Concentrations of volatile (S, Cl) and semi-volatile (F) in parental melts also

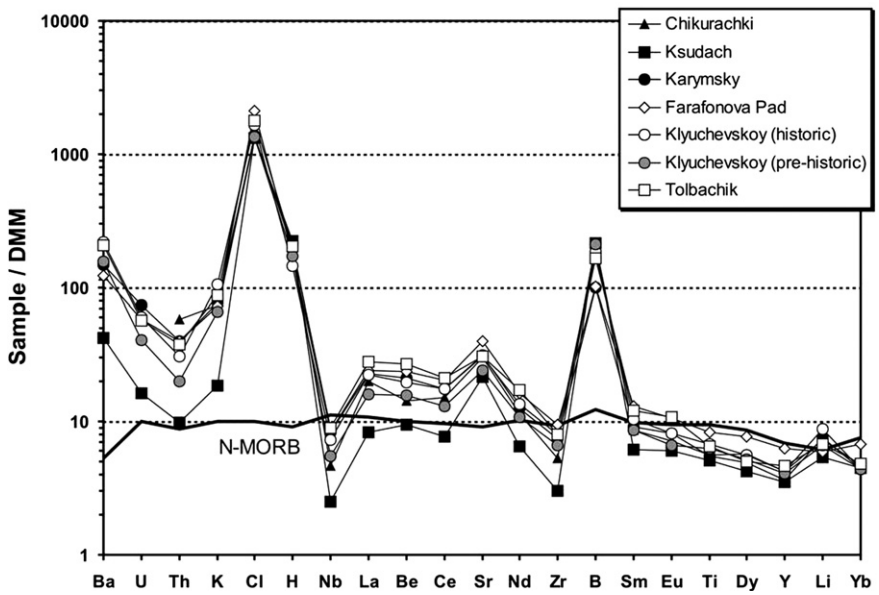

Fig. 2. Volatile and trace elements in parental melts of Kamchatkan volcanoes normalized to the composition of the Depleted MORB Mantle (DMM) [28]. Average composition of N-MORB after [29].

increase with increasing depth to the slab. Variations of Cl (678–1085 ppm) are smaller compared to those of S (773–2720 ppm) and F (100–400 ppm) so that Cl/F (2.3–6.8), Cl/S (0.4–0.9) and ratios of Cl to highly incompatible lithophile elements (e.g., Cl/Nb = 405–1294) are systematically lower in the RA and CKD compared to VF magmas (Fig. 3).

Although there are large variations in the absolute concentrations of highly incompatible elements, there are only small and non-systematic variations of highly incompatible element ratios (e.g., Ba/La, Fig. 3) across the arc. High Ba/La (up to ~50) exceeding those in VF are typical for CKD melts. Ratios of highly incompatible elements to less incompatible elements increase

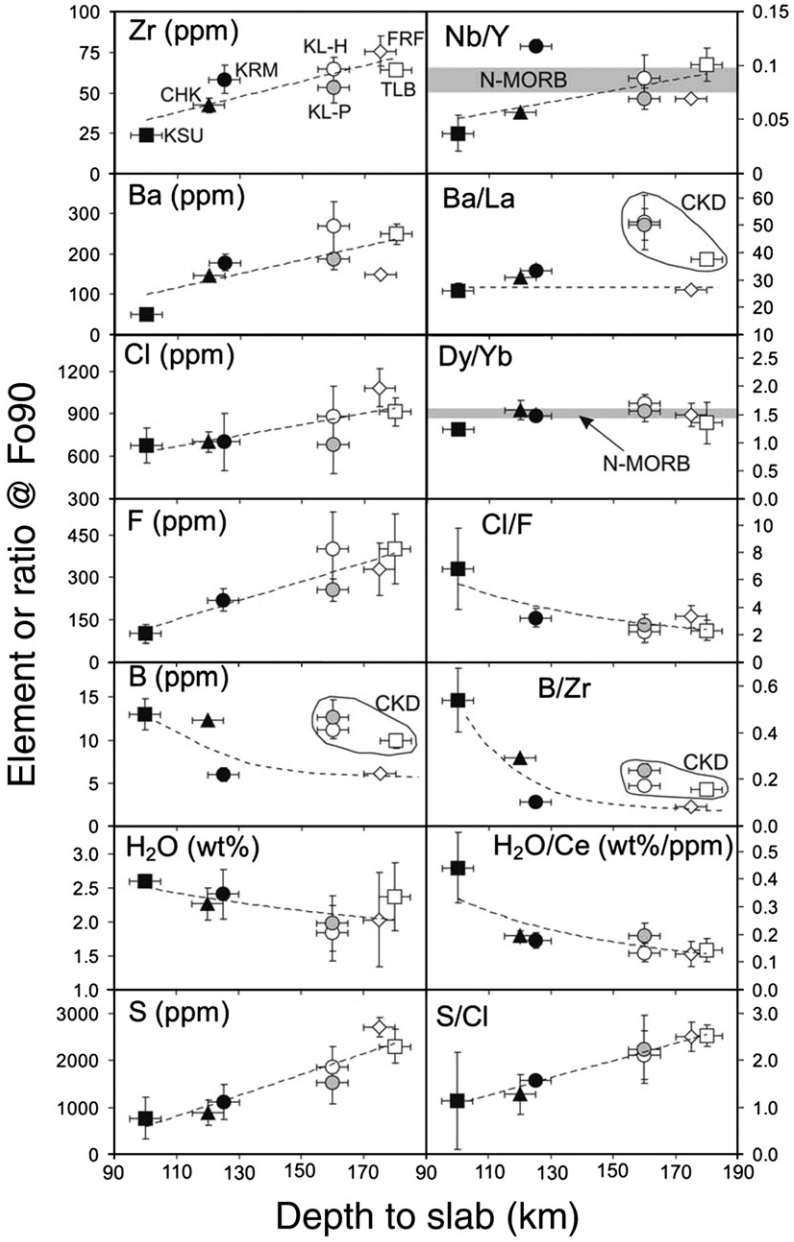

Fig. 3. Volatile and trace elements in mean parental melts of Kamchatka plotted versus depth to the subducting Pacific slab. Composition of N-MORB from [29,30]. Volcano abbreviations: KSU — Ksudach, KRM — Karymsky, CHK — Chikurachki, FRF — Farafonova Pad′, KL-H — Klyuchevskoy (historic), KL-P-Klyuchevskoy (pre-historic), Tolbachik — TLB.

with increasing depth to the subducting slab (e.g., Nb/Y, K_2O/TiO_2, La/Yb) (Fig. 3).

The geochemical systematics of B and H_2O in Kamchatkan magmas is drastically different than for other incompatible elements. Unlike all other trace elements, B concentration and its ratios to incompatible elements (e.g. B/Zr) decrease behind the volcanic front in southern Kamchatka (Fig. 3). Compared to the southern Kamchatka RA, the CKD magmas, generated above a similarly deep subducting slab at 160–180 km, have anomalously high B concentrations (10–13 ppm) and B/Zr (0.15–0.24) similar to VF magmas.

With increasing depth to the slab, maximum H_2O concentrations remain nearly constant (2.5–2.8 wt.%). Mean H_2O concentrations (1.8–2.6 wt.%) tend to decrease from VF to RA (Fig. 3) and exhibit negative correlations with most incompatible elements (e.g. Ba, Ti, Zr, Na, Ti, F) (Fig. 4). Most ratios of H_2O to incompatible elements (e.g., mean $H_2O/Ce = 1556–4400$) decrease and H_2O/B (0.18–0.45) tends to increase from the VF to the RA. H_2O/Ce does not correlate with Ba/Th or any other LILE/HFSE and LILE/REE ratios but forms excellent positive correlations with B/Zr (Fig. 4) and B/LREE and highly concave down negative correlations with ratios of highly incompatible elements relative to less incompatible elements (e.g. Nb/Y or La/Yb).

The negative or lack of correlation between H_2O and incompatible elements in Kamchatkan magmas demonstrates that the use of absolute concentrations of incompatible elements (e.g. K_2O, F, Ba) or their ratios (e.g. Ba/Th) as proxies of water content in arc melts is not straightforward and may lead to erroneous conclusions. The correlation between mean H_2O/Ce and B/Zr in the inclusions indicates that behavior of B and H_2O is to some degree coupled during magma origin in Kamchatka. This correlation however may not be valid for all subduction zones.

5. Modelling of partial melting and composition of slab components

Reasonably well-constrained compositions of parental melts provide an opportunity to examine relationships between extent of partial melting and composition

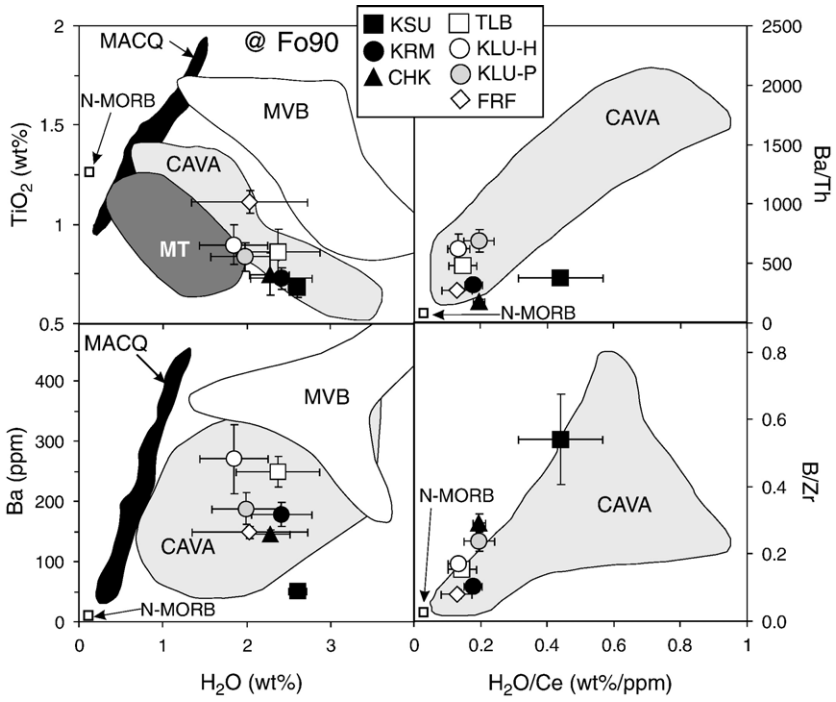

Fig. 4. Correlations of water and trace elements in parental melts. Volcano abbreviations as in Fig. 3. N-MORB composition is after [29], H_2O/Ce and B/Zr in N-MORB after [28]. Melt inclusions from the Central America Volcanic Arc (CAVA) after [20,21,40,41,63] and from the Mexican Volcanic Belt (MVB) after [22]; Mariana Trough (MT) glasses from [3]; E-MORB glasses from Macquarie Island, SW Pacific (MACQ) after [64]. All compositions recalculated to equilibrium with olivine Fo_{90}. Note the positive correlation of H_2O with Ba and TiO_2 in MORB suite from Macquarie Island but negative correlation of H_2O with TiO_2 and lack of clear correlation with Ba for Kamchatka, CAVA, MVB and MT, indicating different regimes of melting beneath mid-ocean ridges and in SZ settings.

of Kamchatkan mantle sources and to estimate the composition of slab components that metasomatized these sources prior to or during partial melting. In order to obtain this information, we use an inverse modelling approach, similar to the method described in [3,18]. Partial melting was assumed to be batch and modal which provides a reasonably good approximation of pooled mantle melts produced during polybaric and near fractional melting (e.g. [18]). Melting was assumed to occur in spinel lherzolite facies as indicated by relatively unfractionated Dy/Yb ratios in Kamchatkan arc melts (1.2–1.7), which are fairly similar to MORB (on average ~1.5 [29,30]) (Fig. 3). Bulk partition coefficients appropriate for melting of spinel peridotite were taken from [18,31]. Modelling included several steps: 1) quantification of source compositions prior to SZ metasomatism and melting, 2) estimation of degree of partial melting (F^m), 3) estimation of composition of metasomatized mantle sources, and 4) quantification of the composition and amount of enriched, presumably slab-derived component (SC) in the sources.

5.1. Steps 1 and 2

Based on the low solubility of HFSE (Nb, Zr, Ti), HREE (Dy, Er, Yb) and Y in slab-derived fluids (e.g. [32]), we assumed that the concentrations of these elements in estimated parental melts are entirely derived from the mantle wedge and thus can provide information about the mantle wedge composition and F^m. As illustrated in Figs. 4 and 5, variations of Nb and Y concentrations and Nb/Y ratios in parental Kamchatkan melts cannot be explained by batch partial melting of a single source composition (e.g. DMM [28]) and imply different degrees of melting of sources variably enriched/depleted in Nb compared to DMM. The most Nb-rich source is required to explain Karymsky parental melt with Nb/Y = 0.12 (Fig. 5). This source should be slightly more fertile than DMM (Nb/Y ~ 0.05) from [28] and is better approximated by Enriched DMM (E-DMM in this work, Nb/Y ~ 0.07) from [31]. Other Kamchatkan parental melts originate from more Nb-depleted sources than E-DMM. Following the approach of [18,33], these depleted sources can be modelled in terms of variable depletion due to a previous stage of melting or Previous Melt Extraction (*PME*) from an initially fertile (E-DMM) source, preceeding the main episode of melting and creating a source with lower Nb/Y than the initial mantle. Alternatively, variations in Nb/Y can be described in terms of enrichment of a depleted source by an OIB-like component (e.g. [34]) or mixing of two contrasting mantle sources (e.g. [35]), which can provide an equally good solution for the estimate of the mantle source prior to a major episode of melting.

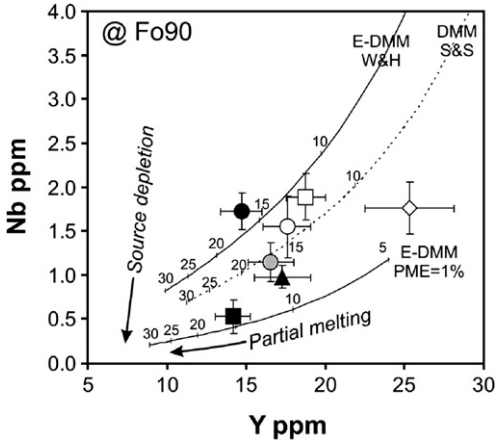

Fig. 5. Variations of Nb and Y in parental magmas. Symbols as in Fig. 3. Solid curves illustrate compositions of melts produced by 30% of batch partial melting of Enriched DMM [31] (labeled as "E-DMM, W and H") and a residue after 1% of previous melt extraction (PME) from E-DMM (labeled as "E-DMM, PME = 1%") calculated by using bulk partition coefficients from [31]. Dashed curve represents compositions of partial melts from DMM [28] calculated by using bulk partition coefficients from [18] (labeled as "DMM, S and S"). Small numbers indicate degree of melting in wt.%.

Following previous workers [36], we applied "PME model" to explain mantle wedge heterogeneity in HFSE. Best-fit amounts of PME from E-DMM and F^m of residual mantle source for every parental melt were found iteratively by searching for minimum residual error of F^m as estimated from 7 incompatible trace elements (Nb, Zr, Ti, Dy, Er, Yb, Y) (Supplementary Fig. 2). Working Excel spreadsheet for these calculations is provided in Supplementary Table 4. The results are shown in Table 1 and Fig. 6 and indicate that variations of fluid-immobile elements in Kamchatkan magmas can be explained by 5–14% partial melting following 0–0.9% PME from a E-DMM-type source. Both F^m and PME were found to decrease with increasing depth to the subducting slab (Fig. 6).

5.2. Steps 3 and 4

Using estimated F^m, the subduction-modified mantle wedge source compositions of Kamchatkan magmas were determined by solving the batch melting equation for all incompatible elements in each parental melt estimated from melt inclusions. An estimate of the incompatible element abundances in an E-DMM source having undergone PME provides an estimate of the source composition before addition of the SC. Comparing the source estimates determined by the two different

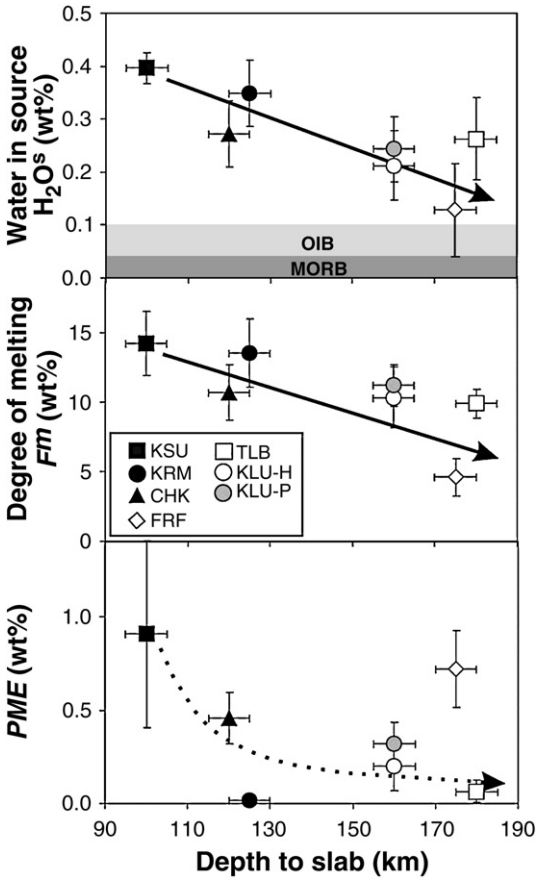

Fig. 6. Mean concentrations of water in mantle sources (H_2O^S), degrees of mantle melting (F^m) and amount of previous melt extraction (PME) for parental melts versus depth to subducting slab. Note high H_2O^S in Kamchatka mantle sources compared to MORB and OIB [9,37–39]. Symbols and volcano abbreviations as in Fig. 3.

methods indicates that all incompatible elements (excluding HFSE and HREE assumed to be derived exclusively from the mantle wedge) are higher in the subduction-modified source than in the E-DMM source having undergone PME. This excess reflects the contribution of SCs to the depleted mantle wedge source. The absolute amount of each element added to the mantle source(s) was calculated, and then the excesses were summarized and normalized to 100 wt.% of oxides [3], providing an estimate for the SC composition and its amount in the source (Table 1). Because our calculations do not account for the presence of all elements in the SC (in particular the major silicate components), the absolute concentrations in the SC should be considered as maximum values and the amount of SC as a minimum value. Ratios of the estimated elements in the SC, however, should reflect the actual ratios of these elements in the SC.

It is important to emphasize that the estimates of PME, F^m, the composition of the subduction modified source (e.g. H_2O^S) and the amount of slab component are dependent on the choice of the initial mantle composition and partition coefficients. For example, using DMM [28] as starting fertile mantle source and a set of partition coefficients from [18] results in systematically higher F^m (by ~3%), H_2O^S (by ~0.05 wt.%) and lower PME (by ~0.5%) for parental melts of Kamchatka compared to our estimates (Supplementary Fig. 3). This discrepancy is relatively small, and results of our study and recent results on back-arc basins from [18] are thus directly comparable. Our results however may drastically differ from results of other studies, particularly when variability of mantle wedge composition and prior melting are not taken into account. The composition of the estimated (silicate-free) slab components is only weakly dependent on the choice of input parameters, especially for elements with large (>90%) contribution from subducted slab (e.g., LILE) [3].

6. Discussion

6.1. Amount of water in Kamchatkan mantle sources

Estimated amounts of H_2O in the sources of Kamchatkan arc-type magmas (H_2O^S) range from ~0.13 wt.% beneath the RA, 0.21–0.26 wt.% beneath the CKD volcanoes, up to 0.4 wt.% beneath the VF (Table 1, Fig. 6). These concentrations are significantly higher than in MORB (80–450 ppm, e.g. [9,37]) and OIB sources (up to 900 ppm, e.g. [38,39]). The Kamchatkan RA and CKD H_2O^S contents overlap with those inferred for back-arc mantle sources (up to 0.38 wt.% for Manus basin [18]) and for the Mexican Volcanic Belt (MVB). They however fall at the lower end of H_2O^S for CAVA as estimated from published data [20–22,40,41] (Fig. 7). Although most estimated concentrations do not exceed the maximum mantle water storage capacity in nominally anhydrous minerals (up to 0.4–0.7 wt.% at 100–200 km depths [42]), the combination of DMM-like source for the Kamchatkan magmas and large excess of water compared to MORB strongly suggests that water was supplied to the Kamchatkan mantle wedge from an external source, that is, from the dehydrating subducting plate.

Causal relationships between the high extent of mantle hydration and the subduction process are strongly supported by the general negative correlation between H_2O^S for Kamchatka (this study) and back-arc [18] magmas with depth to the subducting plate beneath

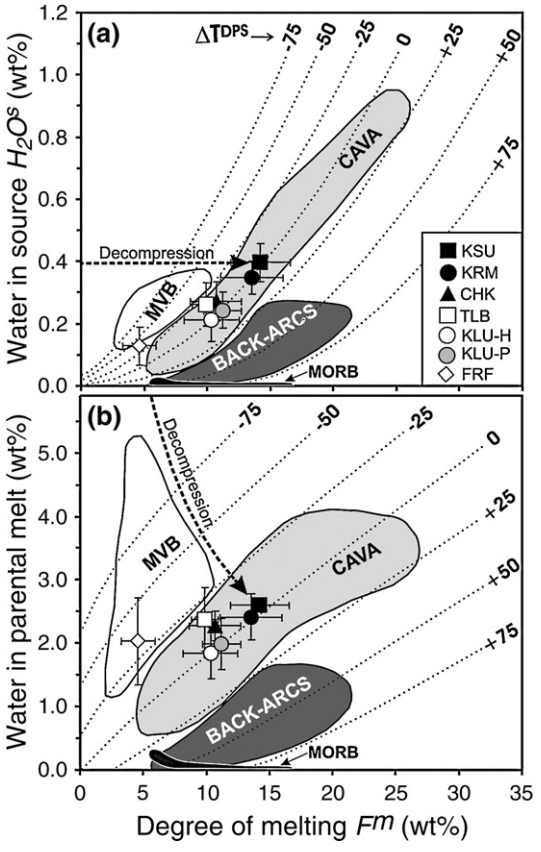

Fig. 7. Relationships between degrees of partial mantle melting (F^m), amount of water in mantle sources (H_2O^S) (figure a) and mean H_2O contents in parental melts of Kamchatka (figure b). Symbols and volcano abbreviations are as in Fig. 3. Dotted curves represent equal deviations from dry peridotite solidus temperatures (ΔT^{DPS}, °C) as calculated after [46] at 1.5 GPa. All melting is water-fluxed at $\Delta T^{DPS} \leq 0$. Some amount of dry melting occurs at $\Delta T^{DPS} > 0$, and its amount is given by intercept of ΔT^{DPS} lines with X-axis (no H_2O in the system). Coefficients at cubic polynomial equations describing H_2O in magmas and sources versus F^m at different ΔT^{DPS} are given in Supplementary Table 5. Melting parameters for Central American Arc (CAVA) and Mexican Volcanic Belt (MVB) were calculated from Ti, Y and H_2O in primitive melt inclusions from [20–22,40,41,63]. Field of back-arc magmas averaged by segment is after [18]. MORB field is drawn by using data on primitive MORB glasses (MgO > 9 wt.%) from [65] and references therein. Thick dashed arrow illustrates compositional evolution of Ksudach parental melt derived from a source with ~0.5 wt.% water rising from deeper and colder parts of mantle wedge through inverted thermal gradient to the zone of magma segregation at shallow depth.

the volcano or distance of the volcanoes from the trench (Fig. 6). This trend is consistent with progressive dehydration of a subducting plate with progressively less water being transferred to the overlying mantle wedge with increasing subduction depth (e.g. [43]) and/or more effective transport of water into the deep mantle in deeper parts of the SZ.

6.2. Constraints on the thermal state of the mantle wedge

The amount of melt produced by hydrous mantle melting depends strongly on temperature; for a given amount of H_2O the degree of melting increases with increasing temperature [18,44–46]. Therefore, estimated H_2O in magmas and their sources and F^m provide an opportunity to assess mantle temperatures beneath Kamchatka, which may correspond to temperatures at which magmas segregate from their mantle residues. To estimate the temperature, we use a parameterized hydrous melting model [46], quantitatively describing relationships between mantle temperature (T), pressure (P), degree of melting (F^m) and bulk amount of water in the system (H_2O^S). Absolute temperature estimates depend on pressures at which the melts are in equilibrium with mantle peridotite, which are difficult to constrain precisely. In order to eliminate the unknown variable P from the working equations in [46], we estimated the temperatures for Kamchatkan mantle sources in terms of temperature deviation (ΔT^{DPS}) to higher or lower values from the 'dry' peridotite solidus $T^{DPS}(P)$ at given pressure: $\Delta T^{DPS} = T(P) - T^{DPS}(P)$, providing a pressure-independent thermometer for parental arc magmas. If P is independently estimated, absolute temperatures can be calculated from ΔT^{DPS} and the equation for $T^{DPS}(P)$, which is well constrained for lherzolite compositions (e.g., $T^{DPS}(P) = 1085.7 + 132.9 \times P - 5.1 \times P^2$ [46]). This thermometer was constrained in coordinates of F^m versus H_2O^S (Fig. 7a) or H_2O in parental melt (Fig. 7b). The later formulation is preferable, because H_2O in melt and F^m are determined independently in practice, whereas H_2O^S is estimated from F^m and H_2O in the parental melt by solving the equation for partial melting [18].

ΔT^{DPS} for Kamchatkan sources estimated from the mean H_2O content in parental melts are close to DPS and range from −30 °C to 0 (Fig. 7), which corresponds to 1245–1330 °C at 1.5–2.0 GPa (sub-crustal depth in Kamchatka). Importantly, the temperature estimates for Klyuchevskoy volcano are fully consistent with the results of liquidus thermobarometry based on major element composition of primitive inclusions in olivine Fo_{90-91} (1280–1320 °C at 1.5–2.0 GPa) [47]. ΔT^{DPS} for VF sources are within error of 0 (DPS) but extend to lower values for the CKD (Tolbachik) and RA (up to −30 °C), indicating that the mantle sources are hotter and/or the pressures (depths) of magma segregation are lower (shallower) beneath the volcanic front in Kamchatka compared to rear arc region.

Mantle temperatures close to and below the DPS suggest that 1) nearly all melting beneath Kamchatka

results from water addition to peridotite in the mantle wedge source, and 2) variable H_2O^S is primarily responsible for the large variations in F^m (Figs. 6 and 7). Although suggested to play an important role in generating arc volcanism, pressure-release 'dry' mantle melting [7,8,32], which occurs above the DPS, is limited by only few percent (if any) in the case of Kamchatka.

Our estimates suggest that regions of magma generation in subduction zones such as Kamchatka, CAVA and MVB are systematically (up to ~100 °C) colder than the mantle beneath mid-ocean ridges and back-arc basins, which undergo substantial melting above the DPS (ΔT^{DPS} = 25–100 °C for MORB and BAB) (Fig. 7). The lower mantle temperatures beneath volcanic arcs compared to ocean ridges and back-arc basins can be qualitatively attributed to the cooling effect of the subducting plate on the overlying mantle wedge. On the other hand, even though significantly lower than in the source for mid-ocean ridge basalts, the mantle wedge temperature beneath volcanic arcs is still higher (up to 300 °C) than expected from isoviscous mantle flow models for SZs (e.g. [48,49]), unless an unrealistically high geothermal gradient (>20 °C/km) is assumed before subduction initiation. Such a high geothermal gradient cannot apply to the Kamchatka Arc, because it is built on relatively thick (30–35 km) continental-type crust. The easiest explanation for the relatively high temperatures beneath volcanic arcs is substantial trenchward oblique mantle upwelling (corner flow associated with some decompression toward the trench) beneath regions of active arc volcanism as predicted by modern SZ models employing non-isoviscous, strong temperature- and stress-dependent olivine rheology [50–52]. In the case of Kamchatka, the non-isoviscous corner flow is thought to be mainly responsible for driving deep and hot mantle from the back-arc region to shallower depths beneath the volcanic arc, with conditions approaching those of the DPS. The addition of variable amounts of water from the subducting slab results in variable amounts of mantle melting.

6.3. The role of lithospheric thickness in arc volcanism

Lithospheric (or crustal) thickness has been proposed to govern partial mantle melting beneath volcanic arcs with the extent of melting increasing as the crust beneath the arc becomes thinner [5]. In order to reconcile decompression and water-flux melting in SZ settings, it was further suggested that the lithospheric thickness mainly influences the amount of 'dry' decompression melting while the amount of water-fluxed melting remains broadly similar for all volcanic arcs [32]. Our data, combined with results on other volcanic arcs having variable crustal thicknesses (Mexican Volcanic Belt, Central America), provide quantitative constraints on this fundamental question pertaining to arc volcanism (Fig. 7).

Water contents and estimated degrees of melting for Kamchatkan, CAVA and MVB volcanic rocks demonstrate that melting beneath these arcs occurs predominantly near or below DPS and thus that water-fluxed melting is the dominant melting process, whereas decompression melting becomes the more important process in the back-arcs (Fig. 7). The amount of flux-melting varies significantly because of local variability in H_2O^S along and across volcanic arcs. The amount of dry decompression melting is limited to <5% and may take place beneath the CAVA. The range of H_2O^S is broadly similar for Kamchatka and MVB (0.1–0.4 wt.%) and extends up to ~1 wt.% for the CAVA. Data for Kamchatka and the CAVA overlap in Fig. 7 indicating similar productivity of flux melting. The MVB data are however displaced to lower F^m suggesting lower productivity of flux melting at lower mantle temperatures (ΔT^{DPS} up to −100 °C) compared to Kamchatka. Crustal thickness is broadly similar in Kamchatka (~35 km) and most parts of the CAVA (30–40 km). The crust is however significantly thicker beneath the MVB (~50 km). Thus, there appears to be a broad negative correlation between crustal thickness and the temperature of magma generation beneath a volcanic arc limiting extent of water-fluxed melting.

We interpret this correlation as evidence for more efficient mantle decompression beneath thinner crust in Kamchatka and CAVA, allowing hot mantle to reach shallower depths and higher productivity of flux-melting compared to MVB, where mantle decompression is limited by thicker crust. As a consequence, we expect greater dry decompression melting (exceeding DPS) beneath intra-oceanic arcs in the West Pacific with crustal thicknesses less than 20–30 km (e.g. Izu-Bonin, Tonga [5,32]). The maximum amount of decompression melting, however, occurs beneath back-arc basins where the crust is thinnest of all (<10 km) [18] (Fig. 7). In conclusion, our findings coincide with the prediction that larger amounts of dry melting occurs beneath thinner arc crust [32] and allow for a fully quantitative estimation of water-flux versus dry melting in SZ settings.

6.4. Composition and nature of slab components

Compositions of the subducting slab components (SC) involved in the genesis of Kamchatkan magmas are highly variable (Table 1, Fig. 8). Concentrations of all elements with the exception of B and Cl correlate

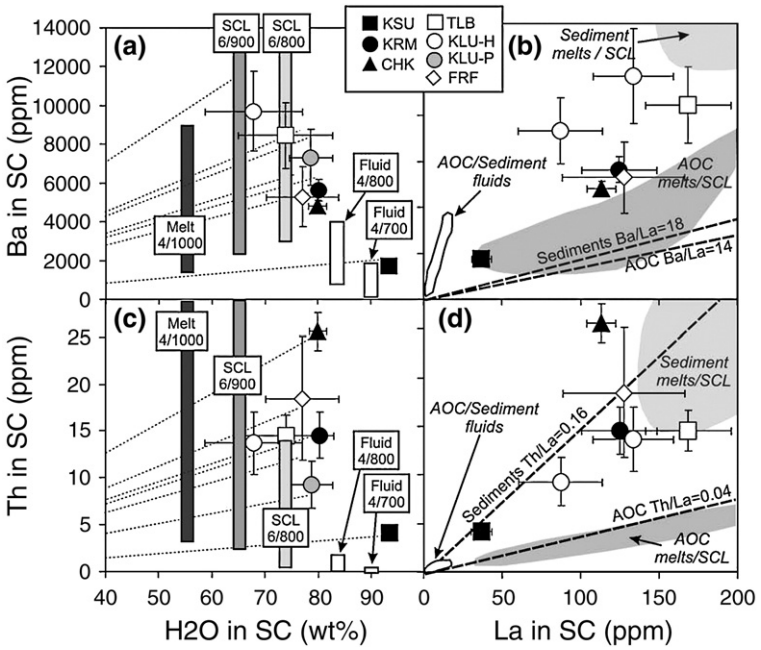

Fig. 8. Variations of H_2O, Ba, Th and La in slab components (SCs). Vertical bars (figures a and c) and shadowed fields (figures b and d) illustrate the compositions of fluids, super critical liquids (SCL) and melts equilibrated with eclogitized altered oceanic crust (AOC) and sediments [66] as calculated by using bulk part partition coefficients and major element compositions of slab fluids and melts at different P–T conditions from [56]. For example, black vertical bar labelled as "Melt 4/1000" in Ba versus H_2O diagram indicates a range of water-saturated melts with $H_2O \sim 55$ wt.% coexisting with eclogitized AOC (lower limit) and sediments (upper limit) at pressure 4 GPa and temperature 1000 °C. Short dashed lines in figures a and c indicate shifting SC compositions with increasing amount of solutes (Si, Al, Na, etc.). Note high Ba and Th concentrations in Kamchatka SCs, which cannot be explained by dehydration or melting of AOC and therefore imply involvement of sediment-derived melts and/or SCL.

negatively with H_2O and tend to increase with increasing depth to slab, while H_2O and B contents decrease, and Cl content remains nearly constant (Supplementary Fig. 4). The most H_2O-rich (>90 wt.%) and trace element-poor (e.g. $K_2O < 5$ wt.%, Th < 5 ppm, La < 50 ppm) SC was estimated for VF Ksudach volcano located at the shortest distance above the subducting plate (~100 km). The SC inferred for volcanic centers (Karymsky, Chikurachki, RA and CKD volcanic rocks) located above a deeper slab (~120–200 km) contain substantially lower H_2O (67–80 wt.%) and higher incompatible element contents (e.g., $K_2O \sim 17$–28 wt.%, Th ~ 9–26 ppm, La ~ 87–169 ppm). Although our estimates of the SC are semi-quantitative and do not take major elements dissolved in the SC in account, these estimates provide important information about 1) the nature of the SC (hydrous fluid and/or melts), 2) the role of hydrous fluids and melts in transporting material from the subducting plate to mantle wedge, and 3) the origin of across-arc zoning.

Water-rich fluids originating at relatively low temperature and pressure ($T \leq 850$ °C, $P \leq 4$ GPa) during dehydration of altered oceanic crust can dissolve substantial amounts of fluid-mobile trace elements (e.g. B, LILE, U, Pb) but are generally expected to be solute poor ($H_2O \geq 80$ wt.%) [53–56]. Experimental data at 4 GPa and temperatures of 700–800 °C [56], for example, suggest low Th (<2 ppm), La (<20 ppm), moderately high Ba (<4000 ppm) and high H_2O/Ba (>0.02 wt.%/ppm) for fluids equilibrated with eclogitized altered oceanic crust and sediments (Fig. 8). The composition of the SC estimated for Ksudach volcano most closely approaches the composition of such solute-poor hydrous fluids; however, some additional contribution from a Th- and LREE-rich component is needed. All other Kamchatkan magmas, including VF magmas (Karymsky and Chikurachki volcanoes), require involvement of a SC which is strongly enriched in the LILE and in elements that are poorly soluble in hydrous fluids (e.g. LREE, Be and Th). On the basis of available experimental data (e.g. [55,56]), we suggest that the SC, which can transport large amounts of LILE, LREE and Th, is most likely a H_2O-rich silicate melt or supercritical liquid with $H_2O/K_2O = 2$–5, H_2O/Ba = 0.02–0.01, Ba/La = 40–80, Th/La = 0.08–0.22. For example, the trace element enriched Kamchatkan SC can either be a hydrous slab melt or represent a mixture of super critical liquids equilibrated with eclogitized basalts and local sediments subducting beneath Kamchatka [56–58] (Fig. 8). Thus, our data indicate transition from hydrous fluid-like to

melt or super critical liquid SC across the Kamchatka arc with increasing depth to the subducting slab, which might be characteristic of volcanic arcs worldwide (e.g. [59,60]). The source of excess amounts of water-rich fluids may be located in deeper parts of the subducting lithosphere (e.g. serpentinites [56,61]), allowing re-equilibration with upper hotter portions of the subducting slab or even causing flash fluid-saturated melting.

The evidence for involvement of melt- or super-critical-liquid-like SC in magma genesis beneath Kamchatka implies that temperatures as high as 700–800 °C, which are required for water-saturated sediment or basalt melting [55], might already be achieved at depths of ~120 km during fast subduction of cold plate, such as the Pacific Plate offshore Kamchatka. Such high temperatures are precluded by isoviscous SZ mantle flow models [48,49], because predicted mantle temperatures are not high enough to significantly heat the subducting plate. In contrast, high mantle wedge temperatures predicted by non-isoviscous flow models, which we favour in our work, have a significant effect on the thermal state of the upper part of the subducting slab which is expected to be hotter, to dehydrate at shallower depths and even to reach the wet sediment and basalt solidus at ~120 km depths [50–52,62]. The changing composition of SC with increasing slab depth is likely a major factor, together with H_2O^S, PME and F^m (Fig. 6), causing across-arc geochemical zonation in the Kamchatka Arc and likely in other volcanic arcs [1,40,60].

Acknowledgments

Authors thank M. Thöner, N. Kononkova and S. Simakin for their help with electron and ion probe analyses; A. Belousov, O. Dirksen, V. Sivorotkin and S. Chirkov for sample donation; G. Avdeiko and O. Khleborodova for field and logistic support in Kamchatka; A. Sobolev and G. Yogodzinski for useful discussion. This work was greatly improved through insightful comments from T. Plank, P. Asimow and three anonymous reviewers on this and a previous version of this manuscript. We gratefully acknowledge broad-based financial support for this project, coming from the German DFG (SFB574, this is contribution number 96; HO1833-14) and BMBF (KOMEX II) and the Russian RFBR (06-05-64873-a).

Appendix A. Supplemtary data

Supplementary data associated with this article can be found, in the online version, at doi:10.1016/j.epsl.2006.12.005.

References

[1] J.B. Gill, Orogenic Andesites and Plate Tectonics, Springer-Verlag, Berlin-Heidelberg, 1981 390 pp.
[2] M.T. McCulloch, J.A. Gamble, Geochemical and geodynamical constraints on subduction zone magmatism, Earth Planet. Sci. Lett. 102 (1991) 358–374.
[3] E. Stolper, S. Newman, The role of water in the petrogenesis of Mariana Trough magmas, Earth Planet. Sci. Lett. 121 (3–4) (1994) 293–325.
[4] J.M. Eiler, A. Crawford, T. Elliott, K.A. Farley, J.W. Valley, E.M. Stolper, Oxygen isotope geochemistry of oceanic-arc lavas, J. Petrol. 41 (2) (2000) 239–256.
[5] T. Plank, C.H. Langmuir, An evaluation of the global variations in the major element chemistry of arc basalts, Earth Planet. Sci. Lett. 90 (1988) 349–370.
[6] J.A. Pearce, P.E. Baker, P.K. Harvey, I.W. Luff, Geochemical evidence for subduction fluxes, mantle melting and fractional crystallization beneath the south sandwich island arc, J. Petrol. 36 (4) (1995) 1073–1109.
[7] T.W. Sisson, S. Bronto, Evidence for pressure-release melting beneath magmatic arcs from basalt at Galunggung, Indonesia, Nature 391 (1998) 883–886.
[8] M.B. Baker, T.L. Grove, R. Price, Primitive basalts and andesites from the Mt. Shasta region, N. California: products of varying melt fraction and water content, Contrib. Mineral. Petrol. 118 (1994) 111–129.
[9] A.V. Sobolev, M. Chaussidon, H_2O concentrations in primary melts from island arcs and mid-ocean ridges: implications for H_2O storage and recycling in the mantle, Earth Planet. Sci. Lett. 137 (1996) 45–55.
[10] P.J. Wallace, Volatiles in subduction zone magmas: concentrations and fluxes based on melt inclusion and volcanic gas data, J. Volcanol. Geotherm. Res. 140 (1–3) (2005) 217–240.
[11] A. Gorbatov, V. Kostoglodov, G. Suarez, E. Gordeev, Seismicity and structure of the Kamchatka subduction zone, J. Geophys. Res. 102 (B8) (1997) 17833–17898.
[12] S.P.e. Fedotov, Active volcanoes of Kamchatka, 302 (V.1) 415 (V.2) pp., Nauka, Moscow, 1991.
[13] O.N. Volynets, Geochemical types, petrology, and genesis of the late Cenozoic volcanic rocks from the Kurile–Kamchatka island-arc system, Int. Geol. Rev. 36 (4) (1994) 373–403.
[14] A.A. Gurenko, A.B. Belousov, R.B. Trumbull, A.V. Sobolev, Explosive basaltic volcanism of the Chikurachki Volcano (Kurile arc, Russia): insights on pre-eruptive magmatic conditions and volatile budget revealed from phenocryst-hosted melt inclusions and groundmass glasses, J. Volcanol. Geotherm. Res. 147 (2005) 203–232.
[15] L. Danyushevsky, A.W. McNeill, A.V. Sobolev, Experimental and petrological studies of melt inclusions in phenocrysts from mantle-derived magmas: an overview of techniques, advantages and complications, Chem. Geol. 183 (2002) 5–24.
[16] L.V. Danyushevsky, F.N. Della-Pasqua, S. Sokolov, Re-equilibration of melt inclusions trapped by magnesian olivine phenocrysts from subduction-related magmas: petrological implications, Contrib. Mineral. Petrol. 138 (2000) 68–83.
[17] L.V. Danyushevsky, A.V. Sobolev, Ferric-ferrous ratio and oxygen fugacity calculations for primitive mantle-derived melts: calibration of an empirical technique, Mineralogy and Petrology 57 (3–4) (1996) 229–241.
[18] K. Kelley, T. Plank, T.L. Grove, E. Stolper, S. Newman, E. Hauri, Mantle melting as a function of water content beneath back-arc

basins, J. Geophys. Res. 111 (B09208) (2006), doi:10.1029/2005JB003732.
[19] J. Blundy, K. Cashman, M. Humphrys, Magma heating by decompression-driven crystallization beneath andesite volanoes, Nature 443 (2006) 76–80.
[20] K. Roggensack, R.L. Hervig, S.B. McKnight, S.N. Williams, Explosive basalic volcanism from Cerro Negro volcano: influence of volatiles on eruptive style, Science 277 (September 12 1997) 1639–1642.
[21] J.A. Wade, T. Plank, W.G. Melson, G.J. Soto, E. Hauri, The volatile content of magmas from Arenal volcano, Costa Rica, J. Volcanol. Geotherm. Res. 157 (2006) 94–120.
[22] P. Cervantes, P.J. Wallace, Role of H2O in subduction-zone magmatism: new insights from melt inclusions in high-Mg basalts from central Mexico, Geology 31 (3) (2003) 235–238.
[23] E. Roedder, Fluid inclusions, Miner. Soc. Amer. Book Crafters Inc., Michigan, 1984, 644 pp.
[24] A.V. Sobolev, Melt inclusions in minerals as a source of principal petrological information, Petrology 4 (1996) 209–220.
[25] D. Massare, N. Metrich, R. Clocchiatti, High-temperature experiments on silicate melt inclusions in olivine at 1 atm: inference on temperatures of homogenization and H_2O concentrations, Chem. Geol. 183 (2002) 87–98.
[26] E. Hauri, J. Wang, J.E. Dixon, P.L. King, C. Mandeville, S. Newman, SIMS analysis of volatiles in silicate glasses 1. Calibration, matrix effects and comparisons with FTIR, Chem. Geol. 183 (2002) 99–114.
[27] V.S. Kamenetsky, S.M. Eggins, A.J. Crawford, D.H. Green, M. Gasparon, T.J. Falloon, Calcic melt inclusions in primitive olivine at 43oN MAR: evidence for melt-rock reaction/melting involving clinopyroxene-rich lithologies during MORB generation, Earth Planet. Sci. Lett. 160 (1998) 115–132.
[28] V.J.M. Salters, A. Stracke, Composition of the depleted mantle, Geochem. Geophys. Geosyst. 5 (5) (2004) Q05004, doi:10.1029/2003GC000597.
[29] S.-S. Sun, W.F. McDonough, Chemical and isotopic systematics of oceanic basalts: implications for mantle composition and processes, in: A.D. Saunders, M.J. Norry (Eds.), Magmatism in the Ocean Basins, Geological Society Special Publication, London, vol. 42, 1989, pp. 313–345.
[30] A.W. Hofmann, Chemical differentiation of the Earth: the relationship between mantle, continental crust and oceanic crust, Earth Planet. Sci. Lett. 90 (1988) 297–314.
[31] R.K. Workman, S.R. Hart, Major and trace element composition of the depleted MORB mantle (DMM), Earth Planet. Sci. Lett. 231 (1–2) (2005) 53–72.
[32] J.A. Pearce, D.W. Peate, Tectonic implications of the composition of volcanic arc magmas, Annu. Rev. Earth Planet. Sci. 23 (1995) 251–285.
[33] J.A. Pearce, I.J. Parkinson, Trace element models for mantle melting: application to volcanic arc petrogenesis, in: H.M. Prichard, T. Alabaster, N.B. Harris, C.R. Neary (Eds.), Magmatic Processes and Plate Tectonics, Geological Society Special Publication, vol. 76, 1993, pp. 373–403.
[34] T. Churikova, F. Dorendorf, G. Worner, Sources and fluids in the mantle wedge below Kamchatka, evidence from across-arc geochemical variation, J. Petrol. 42 (8) (2001) 1567–1593.
[35] M.J. Carr, M.D. Feigenson, E.A. Bennett, Incompatible element and isotopic evidence for tectonic control of source mixing and melt extraction along the Central American arc, Contrib. Mineral. Petrol. 105 (1990) 369–380.
[36] A.G. Hochstaedter, P. Kepezhinskas, M. Defant, M. Drummond, A. Koloskov, Insights into the volcanic arc mantle wedge from magnesian lavas from the Kamchatka arc, J. Geophys. Res., [Solid Earth] 101 (B1) (1996) 697–712.
[37] P.J. Michael, The concentration, behavior and storage of H_2O in the suboceanic upper mantle: Implications for mantle metasomatism, Geochim. Cosmochim. Acta 52 (1988) 555–566.
[38] J.E. Dixon, D.A. Clague, P. Wallace, R. Poreda, Volatiles in alkalic basalts from the North Arch Volcanic Field, Hawaii: extensive degassing of deep submarine-erupted alkalic series lavas, J. Petrol. 38 (1997) 911–939.
[39] A.R.L. Nichols, M.R. Carroll, A. Hoskuldsson, Is the Iceland hot spot also wet? Evidence from the water contents of undegassed submarine and subglacial pillow basalts, Earth Planet. Sci. Lett. 202 (1) (2002) 77–87.
[40] J.A. Walker, K. Roggensack, L.C. Patino, B.I. Cameron, O. Matias, The water and trace element contents of melt inclusions across an active subduction zone, Contrib. Mineral. Petrol. 146 (2003) 62–77.
[41] K. Roggensack, Unraveling the 1974 eruption of Fuego volcano (Guatemala) with small crystals and their young melt inclusions, Geology 29 (10) (2001) 911–914.
[42] M.M. Hirschmann, C. Aubaud, A.C. Withers, Storage capacity of H_2O in nominally anhydrous minerals in the upper mantle, Earth Planet. Sci. Lett. 236 (1–2) (2005) 167–181.
[43] M.W. Schmidt, S. Poli, Experimentally based water budgets for dehydrating slabs and consequences for arc magma generation, Earth Planet. Sci. Lett. 163 (1998) 361–379.
[44] K. Hirose, T. Kawamoto, Hydrous partial melting of lherzolite at 1 GPa: the effect of H_2O on the genesis of basaltic magmas, Earth Planet. Sci. Lett. 133 (1995) 463–473.
[45] M.M. Hirschmann, P.D. Asimov, M.S. Ghiorso, E.M. Stolper, Calculation of peridotite partial melting from thermodynamic models of minerals and melts. III. Controls on isobaric melt production and the effect of water on melt production, J. Petrol. 40 (5) (1999) 831–851.
[46] R.F. Katz, M. Spiegelman, C.H. Lagmuir, A new parameterization of hydrous mantle melting, Geochem. Geophys. Geosyst. 4 (9) (2003) 1073, doi:10.1029/2002GC000433.
[47] S.A. Hubunaya, A.V. Sobolev, Primary melts of calc-alkaline magnesian basalts of Klyuchevskoy volcano (Kamchatka), Dokl. Akad. Sci. 360 (1) (1998) 100–102 (in Russian).
[48] J.H. Davies, D.J. Stevenson, Physical model of source region of subduction zone volcanics, J. Geophys. Res. 97 (B2) (1992) 2037–2070.
[49] S.M. Peacock, T. Rushmer, A.B. Thompson, Partial melting of subducting oceanic crust, Earth Planet. Sci. Lett. 121 (1–2) (1994) 227–244.
[50] P.E. van Keken, B. Kiefer, S.M. Peacock, High resolution models for subduction zones: implications for mineral dehydration reactions and the transport of water into deep mantle, Geochem. Geophys. Geosyst. 3 (2002).
[51] S.M. Peacock, P.E.v. Keken, S.D. Holloway, B.R. Hacker, G.A. Abers, R.L. Fergason, Thermal structure of the Costa Rica — Nicaragua subduction zone, Phys. Earth Planet. Inter. 149 (1–2) (2005) 187–200.
[52] V.C. Manea, M. Manea, V. Kostoglodov, G. Sewell, Thermal models, magma transport and velocity anomaly estimation beneath Southern Kamchatka (Chapter 31), in: G.R. Foulger, D.L. Anderson, J.H. Natland, D.C. Presnall (Eds.), Plates, Plumes and Paradigms, Geological Society of America Special Paper, vol. 388, 2005, pp. 517–536.

[53] H. Keppler, Constraints from partitioning experiments on the composition of subduction-zone fluids, Nature 380 (1996) 237–240.

[54] J.M. Brenan, H.F. Shaw, F.J. Reyrson, D.L. Phinney, Mineral-aqueous fluid partitioning of trace elements at 900 °C and 2.0 GPa: constraints on the trace element chemistry of mantle and deep crustal fluids, Geochim. Cosmochim. Acta 59 (16) (1995) 3331–3350.

[55] M.C. Johnson, T. Plank, Dehydration and melting experiments constrain the fate of subducted sediments, Geochem. Geophys. Geosyst. 1 (1999) (Paper number 1999GC000014. Dec. 13, 1999).

[56] R. Kessel, M.W. Schmidt, P. Ulmer, T. Pettke, Trace element signature of subduction-zone fluids, melts and supercritical liquids at 120–180 km depth, Nature 437 (29 September 2005) 724–727.

[57] T. Plank, Constraints from thorium/lanthanum on sediment recycling at subduction zones and the evolution of the continents, J. Petrol. 46 (5) (2005) 921–944.

[58] S. Duggen, M. Portnyagin, J. Baker, D. Ulfbeck, K. Hoernle, D. Garbe-Schönberg, N. Grassineau, Drastic shift in lava geochemistry in the volcanic-front to reararc region of the Southern Kamchatkan subduction zone: Evidence for the transition from slab surface dehydration to sediment melting, Geochimica et Cosmochimica Acta (2006), doi:10.1016/j.gca.2006.09.018.

[59] J.A. Hoogewerff, M.J. Van Bergen, P.Z. Vroon, J. Hertogen, R. Wordel, A. Sneyers, A. Nasution, J.C. Varekamp, H.L.E. Moens, D. Mouchel, U-series, Sr–Nd–Pb isotope and trace-element systematics across an active island arc-continent collision zone: implications for element transfer at the slab-wedge interface, Geochim. Cosmochim. Acta 61 (5) (1997) 1057–1072.

[60] J.G. Ryan, J. Morris, F. Tera, W.P. Leeman, A. Tsvetkov, Cross-arc geochemical variations in the Kurile Arc as a function of slab depth, Science 270 (5236) (1995) 625–627.

[61] L. Ruepcke, J. Phipps Morgan, M. Hort, J.A.D. Connolly, Are the regional variations in Central American arc lavas due to differing basaltic versus peridotitic slab sources of fluids? Geology 30 (11) (2002) 1035–1038.

[62] P.B. Kelemen, K. Hangøj, A.R. Greene, One view of the geochemistry of subduction-related magmatic arcs, with and emphasis on primitive andesite and lower crust, Treatise on Geochemistry, vol. 3, Elsevier, 2003, pp. 593–659.

[63] S.J. Sadofsky, K. Hoernle, P. van den Bogaard, M. Portnyagin, Subducted Water beneath Central America: How Does Output Vary Along the Volcanic Front? Contributions to Mineralogy and Petrology, submitted for publication.

[64] V.S. Kamenetsky, J.L. Everard, A.J. Crawford, R. Varne, S.M. Eggins, R. Lanyon, Enriched end-member of primitive MORB melts: petrology and geochemistry of glasses from Macquarie island (SW Pacific), J. Petrol. 41 (3) (2000) 411–430.

[65] L.V. Danyushevsky, S.M. Eggins, T.J. Falloon, D.M. Christie, H_2O abundance in depleted to moderately enriched mid-ocean ridge magmas; Part I: incompatible behaviour, implications for mantle storage, and origin of regional variations, J. Petrol. 41 (8) (2000) 1329–1364.

[66] T. Plank, C.H. Langmuir, The chemical composition of subducting sediment and its consequences for the crust and mantle, Chem. Geol. 143 (1998) 325–394.